Nuclear Physics B275 [FS17] (1986) 617–640
North-Holland, Amsterdam

SCALING PROPERTIES OF RANDOMLY TRIANGULATED PLANAR RANDOM SURFACES: A numerical study

A. BILLOIRE[1,2]

Supercomputer Computations Research Institute, Florida State University, Tallahassee, Florida, USA

F. DAVID[3]

Service de Physique Théorique, DPhG, CEN Saclay, 91191 Gif-sur-Yvette Cedex, France

Received 9 June 1986

Results of Monte Carlo simulations of a model of random surfaces based on planar random triangulations with gaussian embedding in D-dimensional euclidean space are presented, for various positive and negative values of D and various forms for the action. Estimates are given for the fractal dimension (Hausdorff dimension of the embedding) and the spreading dimension (intrinsic Hausdorff dimension). The scaling properties appear to depend on the short-distance properties of the triangulations and seem to be nonuniversal, at least for positive D.

1. Introduction

One of the reasons for studying random surface models is to understand what is the meaning of functional integration over geometrical objects, and whether nonperturbative discretization procedures, so successful for local field theories, may be applied to such problems. The following issues are of course of great importance for string theories and for quantum gravity. Is there a natural way to discretize the sum over (two-dimensional) geometries? Is it possible to recover a continuum limit and reparametrization invariance? Do the critical properties of such objects depend on the discretization procedure? The two-dimensional case of random surfaces appears to be the simplest one where such issues may be considered and, up to now, the only one where discrete theories may be compared to exact and analytical results, in particular from string theories.

[1] On leave from Service de Physique Théorique, CEN Saclay, France.

[2] Supported by the Florida State University Supercomputer Computations Research Institute which is partially funded by the US Department of Energy through Contract No. DE-FC05-85ER250000.

[3] Physique Théorique, CNRS, France.

0619-6823/86/$03.50

An interesting class of models of random surfaces, which was recently proposed in [1–3], involves random triangulations. The basic idea is to discretize the sum over 2-dimensional riemannian metrics $\{g_{\mu\nu}(\xi)\}$ over a manifold M by a sum over triangulations T of M, or more precisely a 2-dimensional simplicial complex homeomorphic to M (i.e. with the same topology, characterized by its Euler characteristic χ or its genus g). In its simplest version the intrinsic metric on each triangulation T is frozen so that each link has the same length and each triangle is equilateral, in which case to each triangulation T corresponds only one locally flat riemannian metric on M. If some universality holds, it is expected that this discrete sum over singular metrics will give results similar to the "full" sum over smooth 2-dimensional metrics. Such models can be made into a natural discretization of the Polyakov string model, once the embedding of M in the physical D-dimensional space is realized. Another motivation to study random triangulations comes from "quantum Regge calculus", where one considers a given triangulation T of M, and the intrinsic metric on T varies via the edges lengths. However, one is inexorably led to consider (especially in the strong coupling regime) singular configurations where the triangle inequalities are saturated for some simplices of T, which means that the triangulation chosen is not adequate to study the whole space of metrics and that different triangulations have to be taken into account.

These models of random triangulation have been studied by a large variety of methods: exact solutions [1, 3, 4, 5] based on their duality with some planar field theories, rigorous estimates [2, 6, 7], strong coupling series [8], and computer simulations [4, 9, 10]. The purpose of this paper is to present in detail the results of "microcanonical numerical simulations" of random triangulations embedded in a gaussian way in D-dimensional euclidean space (by microcanonical we mean that the number of vertices of the triangulations is kept fixed, as well as its genus g). The simulations have been performed for various values of the bulk dimension D (including negative ones!) and various forms of the action, and we have looked for various bulk and scaling properties of these random triangulations. A summary account of part of our results has already appeared in [10]. One of the main and novel results of that paper is to present evidence for the nonuniversality of the scaling properties of these random surfaces, which seem to depend continuously on the form of the action.

This paper is organized as follows. In sect. 2 we recall the definition of the model, and define the observables considered. Then we explain the principle of the numerical simulation and give some details on its implementation. In sect. 3 we present results of the simulation for the simplest form of the action for various positive and negative values of the dimension D of bulk space. In sect. 4 we present results for various forms for the action at fixed dimension D. Finally, in sect. 5 we discuss some aspects of our results which have not been considered in the previous sections and draw conclusions.

2. The model and the principle of the Monte Carlo simulation

2.1. DEFINITIONS

A closed triangulation T is defined as a 2-dimensional simplicial complex, i.e. a set of N_2 triangles (2 simplices), N_1 links (1-simplices) and N_0 vertices (0-simplices) such that (i) if a simplex belongs to T, the simplices which belong to its boundary belong to T, and (ii) each link of T belongs to the boundary of exactly two triangles of T.

In fact we shall always consider equivalent classes of triangulations, i.e. identify triangulations T isomorphic by a relabelling of their elements, and use the term triangulation for such classes, when no confusion is possible. Moreover we shall make two important restrictions.

R1. We shall consider *connected planar* triangulations, i.e. triangulations with only 1 connected component and with genus (given by the Euler relation) zero

$$g = -\tfrac{1}{2}(N_2 - N_1 + N_0) + 1 = 0. \tag{2.1}$$

R2. We shall restrict ourselves to triangulations with no loops (i.e. set of links of T forming a loop on T) of length 1 or 2. This means that a link cannot have common extremities and that 2 different links cannot have the same extremities. (See fig. 1.)

Using (2.1) and the relations $3N_2 = 2N_1$ we conclude that N_0, N_1 and N_2 are necessarily of the form

$$N_0 = K + 2, \qquad N_1 = 3K, \qquad N_2 = 2K, \qquad K \geqslant 2 \text{ integer}. \tag{2.2}$$

The simplest case $K = 2$ corresponds to only one triangulation, the tetrahedron. In the following we shall denote by τ_K the set of closed triangulations satisfying conditions R1, R2 and (2.2).

$$\tau_K = \{\text{T: R1, R2 and (2.2) are satisfied}\}. \tag{2.3}$$

Given $\text{T} \in \tau_K$ and some vertex $i \in \text{T}$, the coordination number C_i of the vertex i is trivially defined as

$$C_i = \{\#\text{ of links adjacent to } i\}. \tag{2.4}$$

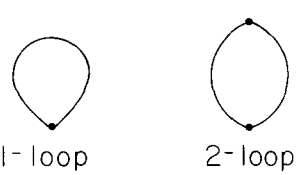

Fig. 1. Loops of length 1 and 2 which are excluded from our configurations by restriction R2.

A discretized version of the curvature density at i is simply*

$$R_i = \pi \frac{6 - C_i}{C_i} . \tag{2.5}$$

The element of the area of i is

$$\sigma_i = \tfrac{1}{3} C_i \tag{2.6}$$

(so that the total area of T is simply N_2). A measure of the flatness of T is provided by the squared curvature.

$$R^2(\mathrm{T}) = \sum_i \sigma_i R_i^2 = \tfrac{1}{3}\pi^2 \sum_i \frac{(6 - C_i)^2}{C_i} . \tag{2.7}$$

Finally, each triangulation is embedded, in a gaussian way, in D-dimensional euclidean space E_d by assigning a vector $X_i \in \mathrm{E}_d$ to each vertex i of T. The Boltzmann factor for each triangulation T of τ_K is defined as

$$W_{\mathrm{T}} = \frac{1}{C(\mathrm{T})} \exp\left[-\gamma R^2(\mathrm{T})\right] \rho(\mathrm{T}) , \tag{2.8}$$

$$\rho(\mathrm{T}) = \int \prod_i^{N_0} \mathrm{d}^D(X_i \sigma_i^\alpha) \exp\left[- \sum_{\text{links } (i,j)} (X_i - X_j)^2 \right] \delta^D(X_{i_0}) , \tag{2.9}$$

where the combinatoric factor $C(\mathrm{T})$ is the order of the symmetry group of T (see [3, 8]) and may be viewed as the remnant in our discretized case of the volume of the gauge orbit (for reparametrization invariance) for two-dimensional gravity. For "typical configurations", $C(\mathrm{T}) = N_0$. The term γR^2 in (2.8) and the term σ_i^α in the measure in (2.9) have the same effect; depending on the sign of γ (or of αD). The probability to have flat vertices with C_i close to 6 increases ($\gamma > 0$) or decreases ($\gamma < 0$) but they correspond, in the naive continuum limit, to irrelevant terms in the action. Their inclusion allows one to probe whether modifications of the short-distance properties of the model change the large-distance (scaling) properties, i.e. if universality holds. The inclusion of the coefficient α in (2.9) has another motivation and two particular cases are interesting.

(i) Conformal measure $\alpha = \frac{1}{2}$. The measure in (2.9) is the natural discretization of the natural functional measure $'\mathscr{D}[X] = \Pi_x \mathrm{d}^D[X|g|^{1/4}]$ on scalar fields in a metric g, which allows one to obtain the conformal anomaly. In our case, the gaussian integration gives

$$\rho(\mathrm{T}) = \left(\tfrac{1}{2}\sqrt{\tfrac{1}{3}}\pi\right)^{(N_0 - 1)D/2} \left[\mathrm{Det}'(-\Delta_0)/N_2\right]^{-D/2} , \tag{2.10}$$

* We use the normalization of [11] for the definition of the scalar curvature on a random lattice.

where Δ_0 is the discretized version of the scalar laplacian [11] on the lattice T, obtained from the connection matrix $[C_{ij}]$ of T

$$C_{ij} = \begin{cases} -1, & \text{if } (i \neq j) \in \text{some link } \ell \in \mathrm{T} \\ N_i, & \text{if } i = j \\ 0, & \text{otherwise} \end{cases}, \tag{2.11}$$

by

$$(\Delta_0)_{ij} = -\sqrt{\tfrac{1}{3}}\,\sigma_i^{-1/2} C_{ij} \sigma_j^{-1/2}, \tag{2.12}$$

and Det′ means the product of the $(N-1)$ nonzero eigenvalues of Δ_0 (the zero mode corresponds to translation and is taken into account by the δ function in (2.9)).

(ii) Flat measure $\alpha = 0$. For this case one has an exact expression for ρ [4, 8]

$$\rho(\mathrm{T}) = (\pi/2)^{(N_0-1)D/2} [\text{number of spanning trees in T}]^{-D/2}. \tag{2.13}$$

Moreover, by considering the lattice T* dual to T one can show that expression (2.10) still holds but now for the scalar laplacian on the dual lattice T* (which is a $N_2 \times N_2$ matrix) or equivalently for the laplacian Δ_2 acting on antisymmetric 2-forms, i.e. pseudoscalar functions, on T. (See [11] for details on differential calculus on a simplicial complex.)

Eq. (2.13) and the duality property described above are the basis of the exact results obtained for $D = 0$ and $D = -2$ [3, 4, 5]. Let us note that with this measure and for $\gamma = 0$ this model is also equivalent to the strong coupling regularization of pure gauge theory proposed in [12] in the planar limit $N_{\text{color}} \to \infty$.

2.2. OBSERVABLES AND SCALING PROPERTIES

Since the Monte Carlo simulations presented here involve triangulations with a fixed number of vertices N_0, we can at best look at scaling properties of the surface. Before detailing the method of the simulation, let us explain the observables we have considered.

2.2.1. Coordination number and squared curvature. First we have considered quantities probing the local structure of the surface, the distribution of the coordination number C_i (2.4) of the vertices and its moments, in particular. The local mean square curvature obtained from (2.7) is

$$\langle r^2 \rangle = \frac{1}{N_2} \langle R^2 \rangle. \tag{2.14}$$

2.2.2. Discrete Liouville action. In order to compare our model to the continuum surface theory of Polyakov [13] we shall measure a discrete version $S_{\mathrm{L}}^{\text{discr}}$ of the

continuum Liouville action S_L

$$S_L = \int d^2\xi \sqrt{g(\xi)} \int d^2\eta \sqrt{g(\eta)}\, R(\xi) \left(\frac{1}{-\Delta} \right)_{\xi,\eta} R(\eta), \tag{2.15}$$

given by a double sum over vertices of T [11, 14]

$$S_L^{\text{discr}} = \sum_i \sum_j R_i \sigma_i^{1/2} R_j \sigma_j^{1/2} (-\Delta_0 + P_0)^{-1}_{ij}, \tag{2.16}$$

where Δ_0 is the scalar laplacian, given by (2.12), and P_0 the projection into the kernel of Δ_0, whose matrix elements are

$$(P_0)_{ij} = \frac{1}{N_2} \sigma_i^{1/2} \sigma_j^{1/2}. \tag{2.17}$$

In the continuum the conformal anomaly gives the linear relation [13] (Λ being the UV cutoff)

$$-\ln \text{Det}'(-\Delta) = \frac{1}{12\pi} S_L + \Lambda^2 \int d^2\xi \sqrt{g} \tag{2.18}$$

and one may look for a similar correlation in the discrete case. We shall find it more convenient to deal with the connection matrix C_{ij} and the projector onto its kernel $(\tilde{P}_0)_{ij} = 1/N_0$ and to consider a slightly modified version of (2.16)

$$\tilde{S}_L^{\text{discr}} = \sum_{ij} (\sigma_i R_i)(C + \tilde{P}_0)^{-1}_{ij} (\sigma_j R_j). \tag{2.19}$$

We leave for the reader the proof of the following relation between $\tilde{S}_L^{\text{discr}}$ and S_L^{discr} (valid for planar triangulations)

$$\tilde{S}_L^{\text{discr}} = \sqrt{3} \left(1 + \frac{4}{N_2} \right)^2 S_L^{\text{discr}} + 16\pi^2 \left(\frac{1 - 2\sqrt{3}}{N_2} - \frac{8\sqrt{3}}{N_2^2} \right). \tag{2.20}$$

2.2.3. Fractal dimension. We now define observables which characterize the scaling exponents of the triangulations. The first one is the mean gyration radius; that is, the mean squared distance in bulk space between two points of the surface

$$\langle X^2 \rangle = \left\langle \frac{1}{N_2^2} \sum_{i,j} \sigma_i \sigma_j (\boldsymbol{X}_i - \boldsymbol{X}_j)^2 \right\rangle. \tag{2.21}$$

It is related to the laplacian $-\Delta_0$ (2.12) for a fixed triangulation T by

$$\langle X^2 \rangle_T = \frac{D}{2\sqrt{3}N_2} \mathrm{Tr}\left[\frac{1}{-\Delta_0 + P_0} - P_0\right], \tag{2.22}$$

or, expressed in terms of the connection matrix (2.11),

$$\langle X^2 \rangle_T = \frac{D}{2N_2}\left\{\left[\sum_i \sigma_i (C_0 + \tilde{P}_0)^{-1}_{ii}\right] - \frac{1}{N_2}\left[\sum_{ij} \sigma_i \sigma_j (C_0 + \tilde{P}_0)^{-1}_{ij}\right]\right\}. \tag{2.23}$$

As for the Liouville action, the projectors onto the zero mode P_0 and $\tilde{P}_0$ have been introduced to define the propagators. The scaling behaviour of $\langle X^2 \rangle$ as $N_2 \to \infty$ defines the fractal dimension d_F, which corresponds to the Hausdorff dimension of the embedding of the random triangulation as

$$d_F = \lim_{N_2 \to \infty} \frac{2 \ln N_2}{\ln\big((1/D)\langle X^2 \rangle\big)}. \tag{2.24}$$

2.2.4. Spreading dimension. The fractal dimension describes the scaling properties of the triangulation in D-dimensional space but one is also interested in scaling properties of the intrinsic geometry of the triangulation T. For instance, one may look at the geodesic distance in T between two vertices (i, j) $d(i, j)$, defined as the minimal length (number of links) of a path joining i to j. The way the average geodesic distance between two vertices, defined by

$$\langle d \rangle = \left\langle \frac{1}{N_0^2} \sum_{ij} d(i, j) \right\rangle, \tag{2.25}$$

scales with N_2 gives a scaling dimension corresponding to some "intrinsic Hausdorff dimension" of the random surface,

$$d_s = \lim_{N_2 \to \infty} \frac{\ln N_2}{\ln \langle d \rangle}. \tag{2.26}$$

Such dimension has in fact already been considered for fractal objects like percolation clusters [15] and is usually denoted by the name of "spreading dimension" (or sometimes "topological dimension").

Other dimension exponents may be considered, like the spectral dimension, which describes the properties of a random walk on T. We shall limit ourselves to d_s because the quantity $\langle d \rangle$ may be measured in a relatively easy way by considering the random walk expansion of a *massive* propagater on a random triangulation T.

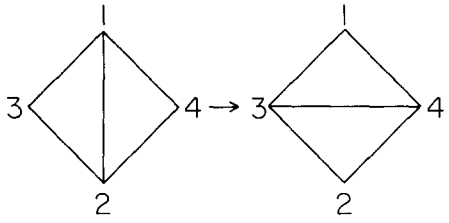

Fig. 2. Elementary flip of a link.

As the mass M^2 goes to infinity, the dominant contribution of the matrix element $(C+M^2)^{-1}_{ij}$ (where C is the connection matrix) is given by the shortest path between i and j, which gives

$$(C+M^2)^{-1}_{ij} \underset{M^2\to\infty}{\simeq} a(M^2)^{-d(i,j)-1}\left(1+\mathrm{O}\left(\frac{1}{M^2}\right)\right), \tag{2.27}$$

where a is some numerical factor, so that

$$d(i,j) = -\lim_{M^2\to\infty}\left\{\frac{\mathrm{d}}{\mathrm{d}\ln M^2}\ln(C+M^2)^{-1}_{ij}\right\} - 1. \tag{2.28}$$

In practice, we shall estimate $\langle d\rangle$ by computing matrix elements of $(C+M^2)^{-1}$ for very large but finite mass M (typically $M^2 = 10^4$).

2.3. PRINCIPLE OF THE MONTE CARLO SIMULATION

The principle of the updating of the configuration is the one proposed in [4]: we change the triangulation by taking a link at random and by flipping this link as represented in fig. 2. In the simplest case where $D=0$ and $\gamma=0$, the Boltzmann weight of a triangulation T is simply the counting factor $1/C(\mathrm{T})$. Then at each step of the simulation the proposed flip is accepted if it does not lead to any excluded configuration (according to rule R2), otherwise it is rejected. It is easy to check that such a process is ergodic (all configurations with fixed genus and fixed number of vertices are reached in that way) and that it respects balance (the simplest way to see that the counting factor $1/C(\mathrm{T})$ is obtained is to consider that the links are labelled, i.e. to consider triangulations instead of classes of triangulation; in that case the counting factor for each triangulation is 1 and it is easy to show that with the process configurations are equiprobable).

When $D=0$, $\gamma\neq 0$ the flip is accepted or rejected according to the change in the action (2.8) by the standard Metropolis procedure.

When $D\neq 0$ one has to update the positions of the vertices. We have used two methods.

Method I. In the first method we perform a separate Monte Carlo for the positions X_i of the vertices i. As in [4] we have used the heat bath algorithm to update the positions of the vertices. During *one iteration* we first update the positions of N_0 randomly chosen vertices (one might perform this operation P times but in practice we have always taken $P = 1$). Then, for fixed positions of the vertices we tried to flip N_1 links chosen at random. The flips are accepted or rejected according to the change in the action (2.8) (depending on the X's, α and γ) by the standard Metropolis procedure. The method works, of course, for integer positive D. The update of the components of the positions is done in parallel, which allows us to go to rather large D's.

Method II. In the second method we compute directly the change in the effective action (2.8), (2.9) during a flip and then accept or reject the flip according to the Metropolis procedure. For the size of surfaces that we have considered, the most efficient method is the Scalapino-Sugar method [16], which consists in storing the full propagator, i.e. in our case the inverse of the connection matrix projected out of the zero mode (which is a $N_0 \times N_0$ matrix)

$$(G_T)_{ij} = (C + \tilde{P}_0)^{-1}_{ij}. \tag{2.29}$$

The flip of fig. 2 may be decomposed in two operations: delete the link (1,2) and add the link (3,4). The exact change in the propagator G_T when one adds a link between two vertices (case $\varepsilon = +1$) or when one suppresses a link (case $\varepsilon = -1$) is given by the formula

$$\Delta G_{ij} = -\frac{\varepsilon}{1 + \varepsilon S}(G_{i1} - G_{i2})(G_{1j} - G_{2j}), \tag{2.30}$$

with

$$S = (G_{11} + G_{22} - 2G_{12}). \tag{2.31}$$

The exact change in the determinant of G (which gives the change in the Boltzmann weight ρ_T) is, for the same operation,

$$\Delta(\det G) = \varepsilon \cdot S \cdot \det G. \tag{2.32}$$

From those formulae the calculation of $\Delta\rho_T$ during a flip requires $\sim N_0^2$ operations, but can of course be vectorized. One limitation is the size of matrix which can be stored in the computer memory. In practice we shall limit ourselves to $N_0 < 10^3$. For such a size of surface, this method for evaluating the propagator appears to be more efficient than statistical methods (which use "pseudofermion" variables [17]) and iterative methods (conjugate-gradient [18]), which have also been tried. These methods are more efficient than the Scalapino-Sugar method if the sparsity of the inverse propagator can be exploited, i.e. if the inverse propagator has

a regular sparsity structure, and if there are much more zero elements than nonzero elements. This is not the case here. Method II is slower than method I but has the advantage of being applicable to negative or noninteger values of D, where of course method I cannot be used. To consider negative bulk dimension D is of interest, in particular to compare our model to the Liouville string theory, which is in the weak-coupling phase for D large and negative. Note that the Boltzmann weight ρ_T and observables such as the mean gyration radius and the fractal dimension d_F are defined for negative D by analytic continuation. In method II during *one iteration* (or sweep) we try to flip N_1 links chosen at random.

During measurement, which occurs after a certain number of sweeps, the quantities are obtained from an exact calculation of the propagator via an inversion algorithm. Let us note that with method I, $\langle X^2 \rangle$ could have been measured directly and that in method II the propagator G is already known exactly at each step. However, an exact calculation does not take too much time and allows us to check that there is no systematic deviation during each run. The statistic has been checked systematically and the error bars estimated using the binning method.

Finally, let us detail the initialization of the system. In all cases we started from a typical configuration at $D = 0$, $\gamma = 0$ obtained by making 10^3 sweeps from some initial configuration. Then, we have made 10^3 sweeps at the final values of D, γ and α before starting the measurements. For large values of D, when using method II, we attempt an adiabatic approach to equilibrium by linearly changing D from 0 to D_{final} during these 10^3 equilibrium sweeps. In the following, the number of sweeps of

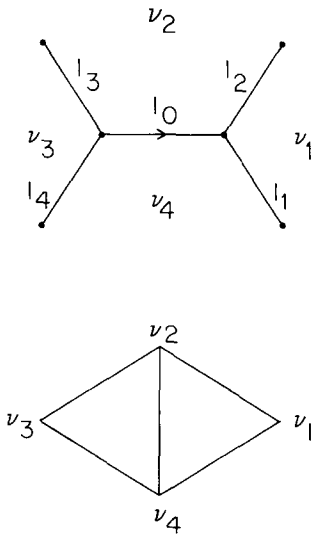

Fig. 3. A link ℓ_0 of the dual lattice T*, its four neighboring links ℓ_i and loops ν_i, and the corresponding original lattice T.

each run denotes the number of measurement sweeps performed after those 2×10^3 equilibrium sweeps.

2.4. LATTICE DESCRIPTION

Finally, let us explain briefly how the information about the random lattice T is stored in the computer. We have found it more convenient to consider both the lattice T and its dual T*, considered as an oriented lattice. (See fig. 3.) To each link of ℓ_0 of T* is associated a table giving the four adjacent links of ℓ_0 in T* $(\ell_1, \ell_2, \ell_3, \ell_4)$ with their orientations, and the four loops of T* (which corresponds to vertices of T) adjacent to ℓ_0 (see fig. 3). This information is sufficient to reconstruct the full connection matrix C_0 of T (which is in fact also stored in order to check the condition (R2) and to reconstruct the neighboring of a given vertex of T). The advantage of dealing with the dual lattice T* is that the coordination number of a vertex is fixed (= 3) instead of varying as for T.

3. Results for $\alpha = 0$, $\gamma = 0$

In this section we present results for simulations performed with the flat measure ($\alpha = 0$) and with no R^2 term ($\gamma = 0$) for various values of the bulk dimension D. A

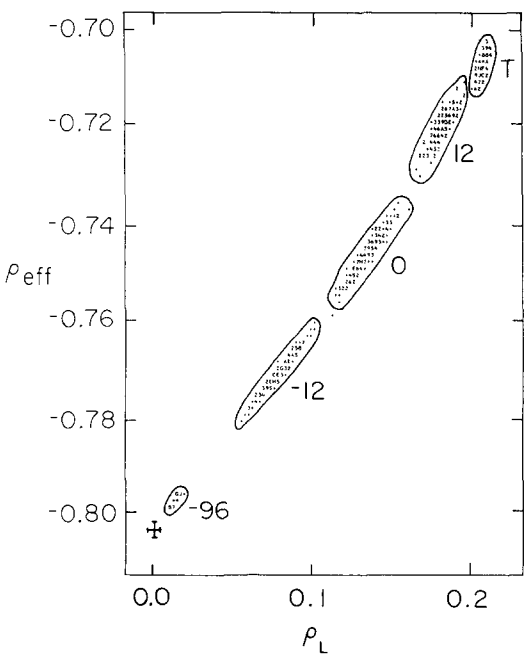

Fig. 4. Scatter plot of the effective action ρ_{eff} versus the Liouville action ρ_L, for $D = -96, -12, 0, 12$ and for tree-like surfaces T ($\alpha = \gamma = 0$).

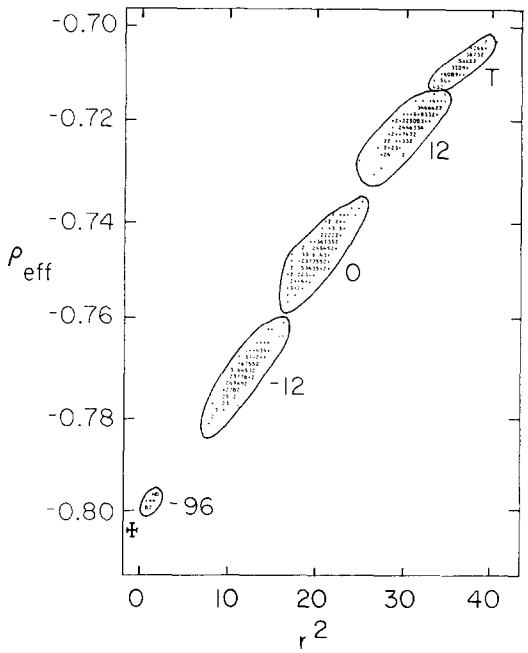

Fig. 5. Scatter plot of the effective action ρ_{eff} versus the squared curvature r^2 for the same configurations.

summary account of the results of this section has already been presented in [10]. The values of D which have been used are $D = 0$, $D = +12$ (where we have used method I) and $D = -12$ and -96 (where we have used method II). The maximal number of vertices N_0 of the triangulation is $N_0 = 128$ for $D = -96$, $N_0 = 256$ for $D = -12$ and $N_0 = 512$ for $D = 0$ and $+12$. During the measurement runs at $D = 0$ and $D = -12$ we have made 5×10^3 iterations and made a measurement each 10 iterations (5×10^2 measurements). For $D = +12$ those numbers are 5×10^4 and 10^2 and for $D = -96$, 2×10^3 and 10. The correlations between successive configurations have been found to increase strongly with the size of the surface (as expected) and with D. This is why we have performed more iterations between each measurement for positive D than for negative D.

3.1. $\langle r^2 \rangle$, LIOUVILLE ACTION AND EFFECTIVE ACTION CORRELATIONS

First we present in figs. 4 and 5 scatter plots of the effective action density

$$\rho_{\text{eff}} = \frac{1}{N_2} \ln \text{Det}(C_0 + \tilde{P}_0), \tag{3.1}$$

with respect to the discretized Liouville action density $\rho_{\text{L}} = (1/N_2)\tilde{S}_{\text{L}}^{\text{discr}}$ and with

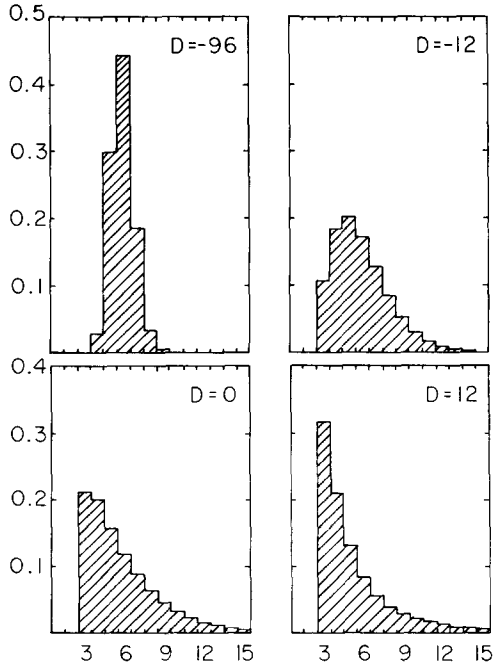

Fig. 6. Histograms of the probability distribution of the coordination number (number of neighbors of a vertex) for the same configurations.

respect to the local mean square curvature $r^2 = (1/N_2)R^2$. On the same figures are represented clusters obtained for samples of 200 surfaces with $N_0 = 128$ vertices obtained for $D = -96, -12, 0, 12$ and for "tree-like surface" (T). Such surfaces are taken as examples of very irregular and curved surfaces, and obtained by a growing process by starting from a tetrahedron ($N_0 = 4$) and by gluing a tetrahedron at random on any triangle of the surface until reaching $N_0 = 128$.

From fig. 5 it is clear that there is a strong and approximately linear correlation between r^2 and the effective action. Since the "temperature" of our system is $-(1/D)$ this means that for large negative D configurations are locally very flat (most of the vertices have coordination number $C_0 = 6$) and that they are more and more irregular with D. This can be seen in fig. 6 where the distribution of coordination numbers is represented. Moreover, for large negative D the configuration seems also to be globally flat, and different for instance from very long "tubes" or polymers (which are also locally flat). Indeed, the crosses in fig. 5 represent the contribution of a flat regular lattice: here a flat torus with the same dimension in the two directions (the change in the topology affects only the low-energy modes of C_0 and therefore should affect the value of ρ_{eff} only by finite size corrections of order $(1/N_2)\ln N_2$). Our data are therefore clear evidence that a flat regular lattice is the global minimum of the effective action. (This was conjectured in [4] but we do not

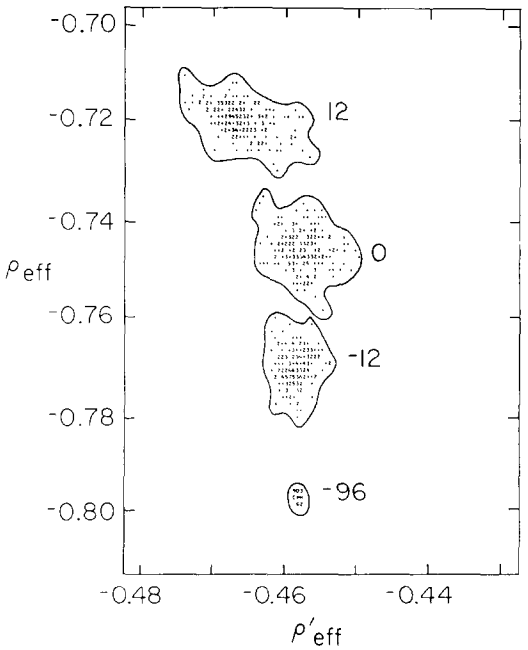

Fig. 7. Scatter plot of the effective action ρ_{eff} versus the logarithm of the determinant of the scalar laplacian ρ'_{eff} for the same configurations.

know any proof of this conjecture.) On the contrary, long polymers, although they have $\langle R^2 \rangle = 0$, have a much larger ρ_{eff}.

From fig. 4 it is clear that there is also a strong linear correlation between the effective action and the discrete Liouville action. We have checked that this correlation persists for larger surfaces at $D = -12$, 0 and 12 and that the width (r.m.s.) of the different observables scales as $N_2^{-1/2}$. The observed correlation is a priori very encouraging. However, the slope obtained from fig. 4 $\delta\rho_{\text{eff}}/\delta\rho_{\text{Liouv}} = s$ is found to be approximately $s \simeq 0.0406$* while the slope obtained in the continuum case is $1/12\pi = 0.0265\ldots$. Moreover (and more importantly) the correlation between ρ_{eff} and R^2 indicates that both the effective action and the regularized Liouville action may depend strongly on the local structure of the surface and therefore on the "high-energy" modes of the laplacian. On the contrary, the form of the effective action (2.18) in the continuum is obtained by integrating out the high-energy modes of the continuum laplacian Δ and therefore rely on the low-energy modes of Δ.

To investigate this issue we have looked at the correlations between $\rho_{\text{L}}^{\text{discr}}$, ρ_{eff} and the effective action obtained from the conformal measure ($\alpha = \frac{1}{2}$), i.e. from the

* There is a normalization error by a factor $\frac{1}{2}$ in [10].

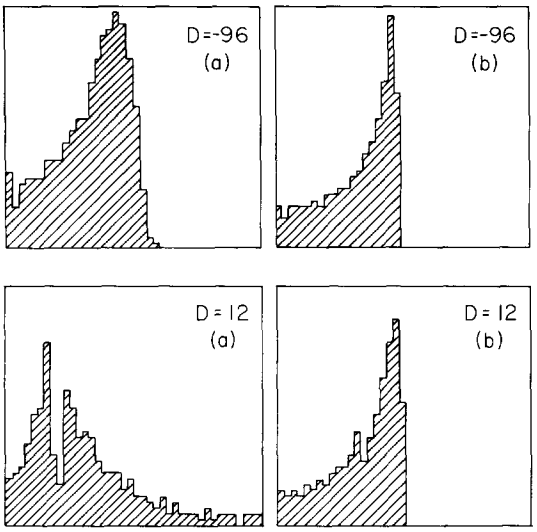

Fig. 8. Histogram of the distribution of eigenvalues of the connection matrix C (a) and of the scalar laplacian $(-\Delta_0)$ (b) for $D=-96$ and $D=12$ (each figure is obtained by averaging 10 different triangulations with $N_0=128$).

scalar laplacian:

$$\rho'_{\text{eff}} = \frac{1}{N_2} \ln \text{Det}(-\Delta_0 + P_0) \tag{3.2}$$

for the configurations generated in our runs.

Contrary to ρ_{eff}, ρ'_{eff} does not seem to depend clearly on D, as illustrated on the scatter plot of fig. 7. A numerical study of the eigenvalues of the two operators C_0 and $-\Delta_0$ (given by (2.11) and (2.12)) for typical triangulations generated reveals the following features (see fig. 8):

(i) The small eigenvalues of C_0 and $(-\Delta_0)$ (i.e. the eigenvalues λ much less than the mean eigenvalue for C_0 (which is $\lambda=6$)) are linearly correlated and therefore should contribute in the same way in ρ_{eff} and ρ'_{eff}.

(ii) On the contrary, the large eigenvalues of C_0 and those of $(-\Delta_0)$ have a very different distribution. There is a sharp cut-off in the distribution of the eigenvalues of $(-\Delta_0)$ at the maximum $\lambda_{\max}=\frac{1}{2}\sqrt{3}$. On the other hand the distribution of the eigenvalues of C_0 is much broader, especially for positive D, and it appears that these large eigenvalues of C_0 are responsible for the correlations described above between ρ_{eff}, r^2 and S_{L}.

Moreover, the form (2.18) for the effective action given by the conformal anomaly is only valid for 2-dimensional surfaces. As we shall see, the effective intrinsic dimensionality of our triangulations, defined by the spreading dimension (2.26) is

TABLE 1
Mean gyration radius $\langle x^2 \rangle$ as a function of N_0 and D, for $\alpha = \gamma = 0$ and corresponding estimates for the fractal dimension d_F

N_0 \ D	−96	−12	0	12
8	0.18448 (1)	0.18565 (3)	0.18592 (3)	0.18573 (4)
16	0.2037 (1)	0.2070 (1)	0.2081 (1)	0.2059 (3)
32	0.2294 (1)	0.2353 (1)	0.2395 (3)	0.2335 (10)
64	0.2580 (1)	0.2659 (3)	0.2769 (6)	0.2621 (13)
128	0.2879 (1)	0.2972 (5)	0.3189 (17)	0.3001 (30)
256		0.3322 (6)	0.3681 (16)	0.3417 (20)
512			0.4216 (33)	0.3996 (42)
d_F	> 13	12.5 (3)	9.9 (4)	9.7 (5)

larger than 2. This is another reason to suspect that the correlation between the discrete Liouville action and the effective action is generated in our case by a different mechanism than the conformal anomaly.

3.2. SCALING DIMENSIONS

We now present our results on the scaling behavior of the gyration radius $\langle x^2 \rangle = (1/D)\langle X^2 \rangle$ (2.22) and of the geodesic distance $\langle d \rangle$ (2.25). The results of the simulations are given in tables 1 and 2. Log-log plots of $\langle x^2 \rangle$ and $\langle d \rangle$ respectively versus the number of vertices N_0 are shown in figs. 9 and 10. Corresponding estimates for the fractal dimension d_F and the spreading dimension d_s, obtained by a linear fit of the points in figs. 9 and 10, are given on the last row of tables 1 and 2 respectively.

TABLE 2
Mean geodesic distance $\langle d \rangle$ as a function of N_0 and D, for $\alpha = \gamma = 0$ and corresponding estimates for the spreading dimension d_s

N_0 \ D	−96	−12	0	12
8	1.0554 (1)	1.0578 (2)	1.0585 (1)	1.0580 (1)
16	1.6188 (6)	1.5947 (9)	1.5913 (9)	1.571 (2)
32	2.350 (2)	2.2464 (8)	2.216 (5)	2.131 (8)
64	3.324 (3)	3.040 (2)	2.954 (5)	2.71 (1)
128	4.623 (4)	4.017 (6)	3.843 (15)	3.40 (3)
256		5.270 (9)	4.940 (22)	4.19 (2)
512			6.32 (5)	5.25 (5)
d_s	< 2.5	2.55 (5)	2.8 (1)	3.2 (2)

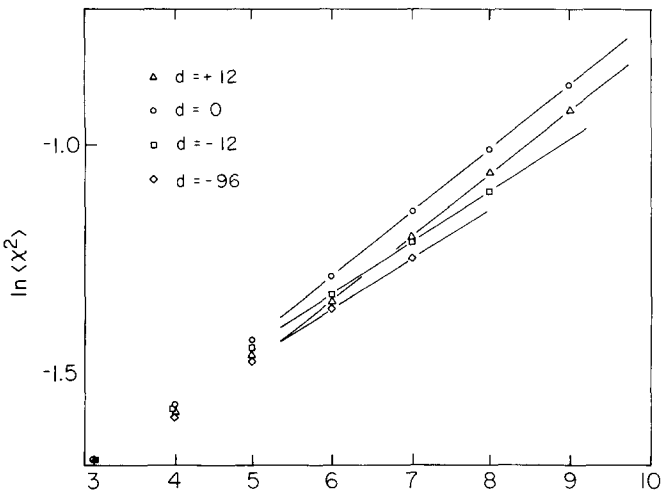

Fig. 9. Log-log plot of the mean square extend $\langle x^2 \rangle$ versus the number of vertices N_0, for $\alpha = \gamma = 0$ and for $D = -96, -12, 0, 12$.

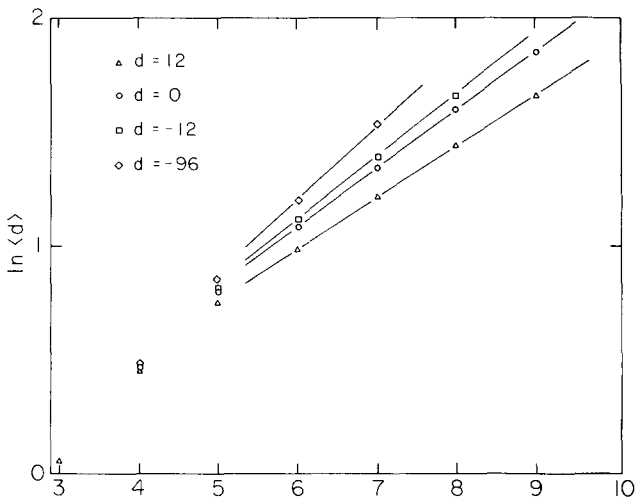

Fig. 10. Log-log plot of the geodesic distance $\langle d \rangle$ versus N_0, for $\alpha = \gamma = 0$ and for $D = -96, -12, 0, 12$.

The growth of $\langle x^2 \rangle$ with N_0 does not depend in a drastic way on the bulk dimension D. For $D = -12$, 0 and $+12$, it seems reasonable to assume from the data that the scaling regime has been reached for $N_0 \geqslant 64$. The fractal dimension is large (~ 10) with perhaps a slight decrease when D increases. The same can be said for $\langle d \rangle$, but for a rather strong increase with D. For $D = -96$, since typical surfaces are very flat, long-range fluctuations are expected to be much more important and for the size of surfaces considered, the scaling region has not yet been reached. However, from the concavity of the plots of figs. 9 and 10, it seems plausible that d_F is large (> 13) and that d_s is smaller than 2.5. This is consistent with the conjecture that flat regular lattices are the dominant configurations at $D = -\infty$, since they give $d_F = \infty$, $d_s = 2$.

We have also performed runs at $D = +48$. Here one seems to get very easily trapped into singular configuration with a few vertices of very large coordination number* and the statistics become very poor. Thus for large D it seems that the surfaces are very irregular, and very different for instance from branched polymers (which dominate for large D for models of random surfaces on regular lattices) which give $d_F = 4$ and $d_s = 2$.

4. Scaling properties for different actions

As we have seen, it seems that the short-distance properties of the surface play an essential role in the effective action and one could expect that the critical properties may depend on these properties. Motivated by these considerations, and by the results of a parallel simulation [9] with a different action which gave different estimates for d_F at large D, we have studied in two cases how the critical properties depend on the exact form of the action, by changing the value of the squared curvature coupling γ and the form of the measure in (2.8), (2.9).

4.1. $D = 12$, $\gamma = 0$, $\alpha \neq 0$

In tables 3 and 4 are presented results at $D = 12$ for three different forms for the measure on the X's, parameterized by the parameter α: $\alpha = 0$ (flat measure previously considered), $\alpha = 0.5$ (conformal measure considered in [9]) and $\alpha = 0.25$ (intermediate case). The number of iterations is the same: 5×10^4, with measurement every 5×10^2 iterations for the largest surface ($N_0 = 512$). As can be seen from tables 3 and 4 and from fig. 11, there is a drastic change in the scaling behaviour of $\langle x^2 \rangle$ and $\langle d \rangle$ for $\alpha = 0.5$. The estimates for d_F and d_s, obtained by a linear fit of the log-log plots, show that they both decrease strongly for large α and moreover that the transition seems to be smooth. The estimates for $\alpha = 0.5$ are much closer to what is expected for branched polymers. These results corroborate those of ref. [9] obtained for positive D with the conformal measure ($\alpha = 0.5$).

* In a recent preprint by Ambjørn, Durhuus, Fröhlich and Orland [19] it has been shown that such configurations in fact dominate in the limit $D = +\infty$.

TABLE 3
$\langle x^2 \rangle$ as a function of α for $D = 12$, $\gamma = 0$

N_0 \ α	0.	0.25	0.5
8	0.18573 (4)	0.1860 (1)	0.1861 (1)
16	0.2059 (3)	0.2112 (5)	0.2145 (5)
32	0.2335 (10)	0.2505 (14)	0.2671 (13)
64	0.2621 (13)	0.3122 (25)	0.3490 (22)
128	0.3001 (30)	0.3941 (40)	0.4646 (46)
256	0.3416 (20)	0.5082 (50)	0.6544 (63)
512	0.3996 (42)		0.8925 (134)
d_F	9.7 (5)	5.5 (1.0)	4.2 (0.5)

TABLE 4
$\langle d \rangle$ as a function of α for $D = 12$, $\gamma = 0$

N_0 \ α	0.	0.25	0.5
8	1.0580 (1)	1.0586 (3)	1.0591 (4)
16	1.571 (2)	1.606 (3)	1.631 (4)
32	2.131 (8)	2.27 (1)	2.404 (10)
64	2.71 (1)	3.16 (2)	3.48 (2)
128	3.40 (3)	4.29 (3)	5.00 (4)
256	4.19 (2)	5.83 (5)	7.19 (6)
512	5.25 (5)		10.08 (14)
d_s	3.2 (2)	2.2 (3)	2.0 (2)

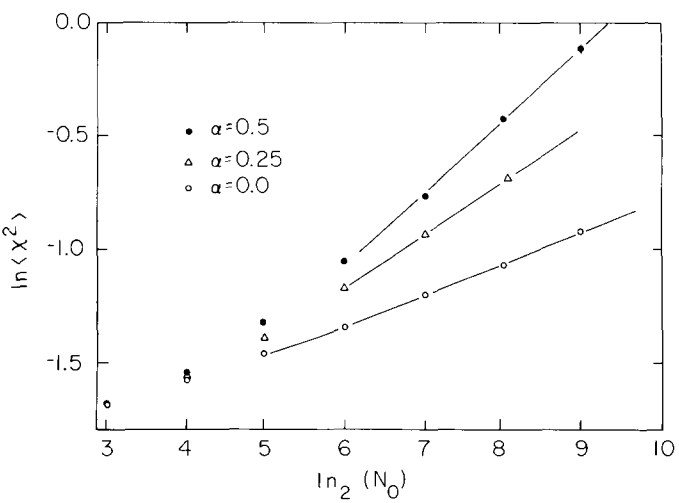

Fig. 11. Log-log plot of $\langle x^2 \rangle$ versus N_0, for $D = 12$ and $\alpha = 0$, 0.25 and 0.5 ($\gamma = 0$).

TABLE 5
$\langle x^2 \rangle$ as a function of $\gamma' = \gamma/(3\pi^2)$ for $D = 0$

N_0 \ γ'	−1.	−0.5	0.	1.	2.
8			0.18592 (3)		
16			0.2081 (1)		
32	0.2084 (5)	0.2198 (4)	0.2395 (3)	0.2562 (7)	0.2436 (12)
64	0.2191 (5)	0.2400 (7)	0.2769 (6)	0.3025 (20)	0.2980 (26)
128	0.2312 (8)	0.2624 (5)	0.3189 (17)	0.3592 (27)	0.3562 (35)
256	0.2448 (8)	0.2845 (10)	0.3681 (16)	0.4309 (26)	0.4299 (47)
512		0.3114 (10)	0.4216 (33)	0.4965 (20)	
d_F	25. (2)	15. (1)	9.9 (4)	9.0 (1)	7.5 (1)

4.2. $D = 0$, $\gamma \neq 0$

We now present a systematic study of the role of the local curvature performed at $D = 0$ for various values of the squared curvature coupling γ. For positive γ locally flat triangulations ($C_i \simeq 6$) are favoured and for negative γ those locally very curved ($C_i \neq 6$) are favoured. In tables 5 and 6 are presented results for $\langle x^2 \rangle$ and $\langle d \rangle$ respectively. Log-log plots are presented in figs. 12 and 13. The number of iterations is 5×10^4 with a measurement after 10^2 iterations. In fact we have used the coupling $\gamma' = \gamma/(3\pi^2)$.

The growth factor of $\langle x^2 \rangle$ and $\langle d \rangle$ with N_0 depends clearly on γ and is larger for positive γ than for negative ones (this corresponds to smaller scaling dimensions). Linear fits for the log-log plot of figs. 12 and 13 give estimates for d_F and d_s presented in the last row of tables 5 and 6.

The fractal dimension d_F is found to be very large for negative γ, but for such values one cannot exclude that it is in fact infinite, and that $\langle x^2 \rangle$ is proportional to $\ln N_0$. For positive γ there seems to be saturation. This is perhaps the signal that for

TABLE 6
$\langle d \rangle$ as a function of $\gamma' = \gamma/(3\pi^2)$ for $D = 0$

N_0 \ γ'	−1.	−0.5	0.	1.	2.
8			1.0585 (1)		
16			1.5913 (9)		
32	1.943 (6)	2.035 (4)	2.216 (5)	2.384 (5)	2.384 (8)
64	2.344 (8)	2.555 (7)	2.954 (5)	3.384 (14)	3.481 (21)
128	2.762 (14)	3.140 (8)	3.843 (15)	4.624 (26)	4.863 (31)
256	3.248 (18)	3.804 (12)	4.940 (22)	6.257 (16)	6.704 (48)
512		4.648 (15)	6.32 (5)	8.186 (23)	
d_s	4.3 (5)	3.5 (3)	2.8 (1)	2.6 (2)	2.2 (3)

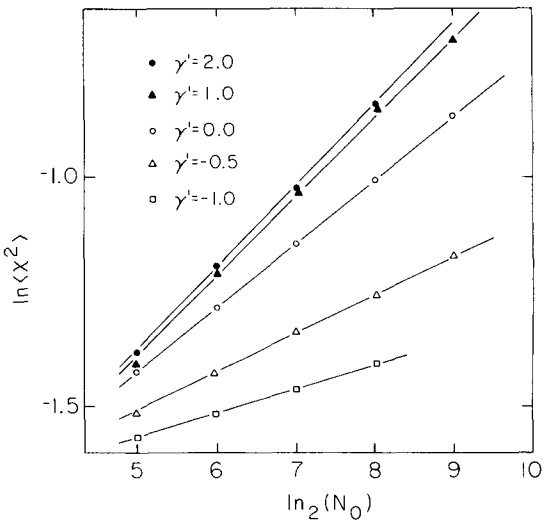

Fig. 12. Log-log plot of $\langle x^2 \rangle$ versus N_0, for $D = 0$, and various $\gamma' = \gamma/3\pi^2$.

very large γ the surface becomes regular and that $d_F = \infty$ (this is only a possibility). For $\langle d \rangle$ the scaling is less clear but there is a systematic decrease of d_s as γ increases and we observe also a saturation of d_s for positive γ (compatible with the scenario suggested above). Finally we present in fig. 14 a scatter plot of the effective action density ρ_{eff} versus the Liouville action density ρ_L for 500 configurations with $N_0 = 512$ for $\gamma = -0.5$, 0. and 1. The slope is the same as in fig. 4.

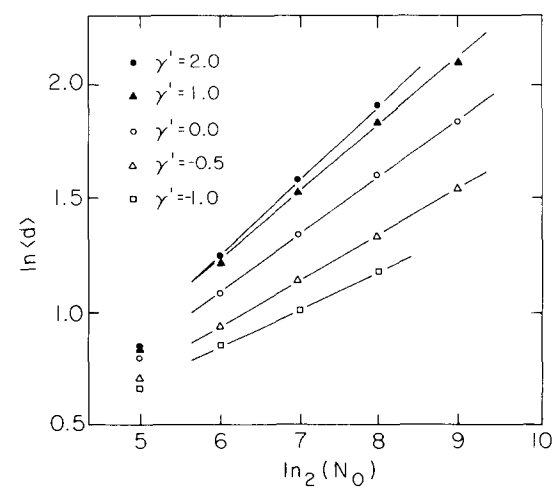

Fig. 13. Log-log plot of $\langle d \rangle$ versus N_0, for $D = 0$, and various $\gamma' = \gamma/3\pi^2$.

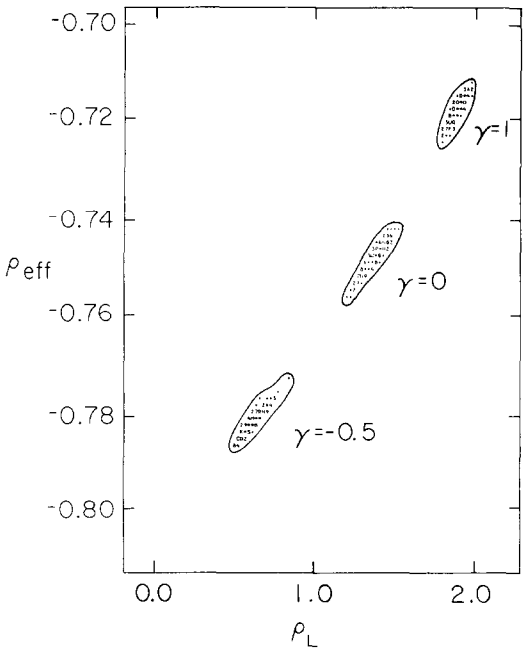

Fig. 14. Scatter plot of ρ_{eff} versus ρ_{L}, for $D = 0$ and various $\gamma' = \gamma/3\pi^2$, ($N_0 \simeq 512$).

5. Discussion and conclusion

What conclusion can one draw from such a study? As we have seen, there is reasonable numerical evidence that for the size of surface considered in our simulation, we have reached a scaling behaviour and may extract estimates for some scaling exponents. However, those scaling properties seem to depend strongly on the discretization of the surface, i.e. from terms in the action (or in the functional measure) which could be expected to be irrelevant (from naive dimensional considerations) in the continuum limit. Of course these arguments are valid only if we are in the vicinity of a gaussian fixed point, which is not the case here. Moreover it is clear that (scalar) fields on those random lattices are strongly coupled to the short-distance geometric excitation of the lattice and may influence the scaling behaviour. Two possibilities may arise:

(a) The scaling behaviour (and in particular the scaling dimensions d_{F} and d_{s}) varies continuously with the form of the action. This means a strong breakdown of the concept of universality for that class of models of random surfaces.

(b) There is a *finite* set of critical behaviours (fixed points) depending on the exact form of the action. The change in the scaling law simply reflects the crossover between at least two different behaviours. However, if the scaling behaviour observed in our simulation is not the real asymptotic one, surfaces larger by at least

one order of magnitude will have to be considered and it seems hopeless to explore this regime by numerical methods in the near future (at least for the class of models considered here).

In this work we have only considered surfaces with a fixed number of triangles. It is necessary also to consider the canonical model by assigning a fugacity $z = e^{-\beta}$ to each triangle and to study the critical behaviour of the model at the critical point β_{cr} beyond which the surface area becomes infinite. Estimates for the associated susceptibility exponent γ (describing how the mean area diverges at β_{cr}) based on high temperature series have been given by one of the authors in [8] for various bulk dimension D. In this study the estimates for γ did not seem to vary too much with the exact form of the action*. It would be useful to get estimates on γ by Monte Carlo simulations where the number of triangles is allowed to vary in order to compare them with the exact results and those from series analysis. Algorithms for such simulations may be constructed [19–21], and some preliminary numerical studies have already been performed, by one of us [20]. It appears that the occurrence of critical fluctuations in the number of triangles near the critical point necessitates very long runs in order to get precise and reliable estimates.

Finally let us discuss which insights the study of random triangulation may give for other problems involving geometrical objects. First of all, as already stressed, the details of the discretization and the short-distance dynamics of the surface is of major importance for the scaling properties of the model. In our opinion, such questions should be equally important in other models of random surfaces, for instance those of refs. [11, 14] relying on the idea of Regge calculus. In particular, the form of the measure chosen for the intrinsic metric should be very carefully analyzed. Those remarks are even more relevant for Regge quantum gravity in space-time dimension $d = 4$ [22–24]. Our understanding of the dynamical issues of these discrete theories is still very poor and the numerical simulations [25, 26] have been made up to now on very small systems. Another important point is that the long-distance properties of objects with fluctuating geometry (for instance here the spreading dimension d_s) are not necessarily related to their properties at the level of the discretization. This is of course not new, as has been learned from the study of critical phenomena, but the significance of this fact for quantum gravity must not be underestimated.

The simulations were performed using the CRAY X-MP/22 at Saclay. We are very grateful to J. Jurkiewicz, A. Krzywicki and B. Petersson for interesting discussions and for communicating to us the results of their simulations prior to publication. We benefited from comments by G. Bhanot and D. Duke on the manuscript. One of us (F.D.) also thanks H. Hermann and J.M. Luck for useful discussions.

* This fact was used to estimate the error bars for γ. Such a procedure is, of course, very questionable if γ is not universal.

Note added

After the completion of this work, we received two preprints by Boulatov, Kazakov, Kostov and Migdal [27] which present analytical and Monte Carlo studies of the model considered here. The results of those numerical simulations are in accordance with ours, as well as with those of [9]. We thank Dr. Kostov for communicating to us those preprints.

References

[1] V.A. Kazakov, Phys. Lett. 150B (1985) 282
[2] J. Fröhlich, *in* Application of field theory to statistical mechanics, Lecture Notes in Physics, vol. 216, ed. L. Garrido (Springer, 1985)
[3] F. David, Nucl. Phys. B259 (1985) 45
[4] V.A. Kazakov, I.K. Kostov and A.A. Migdal, Phys. Lett. 157B (1985) 295
[5] F. David, Phys. Lett. 159B (1985) 303
[6] J. Ambjørn, B. Durhuus and J. Fröhlich, Nucl. Phys. B259 (1985) 433
[7] J. Fröhlich, *in* Recent developments in quantum field theory, Proc. Niels Bohr Centennial Conference (May 6-10, 1985) ed. J. Ambjørn, B.J. Durhuus and J.L. Petersen (North-Holland, 1985)
[8] F. David, Nucl. Phys. B257 (1985) 543
[9] J. Jurkiewicz, A. Krzywicki and B. Petersson, Orsay preprint LPTHE 85/36, Phys. Lett. B, to be published
[10] A. Billoire and F. David, Phys. Lett. 168B (1986) 279
[11] M. Bander and C. Itzykson, *in* Lecture Notes in Physics, vol. 226 (Springer, Berlin, 1985); Nucl. Phys. B257 (1985) 543
[12] J.M. Drouffe, Nucl. Phys. B218 (1983) 89
[13] A.M. Polyakov, Phys. Lett. 103B (1981) 207
[14] A. Jevicki and M. Ninomiya, Phys. Lett. 150B (1985) 115
[15] J. Vannimenus, J.P. Nadal and H. Martin, J. Phys. A17 (1984) L351
[16] D.J. Scalapino and R.L. Sugar, Phys. Rev. Lett. 46 (1981) 519
[17] F. Fucito, E. Marinari, G. Parisi and C. Rebbi, Nucl. Phys. B180 [FS3] (1981) 360
[18] D. Weingarten and D. Petcher, Phys. Lett. 99B (1981) 333
[19] J. Ambjørn, D. Durhuus, J. Fröhlich and P. Orland, Nucl. Phys. B270 [FS16] (1986) 457
[20] F. David, unpublished
[21] J. Jurkiewicz, A. Krzywicki and B. Petersson, private communication
[22] T. Regge, Nuovo Cim. 19 (1961) 558
[23] M. Roček and R. Williams, Phys. Lett. 104B (1981) 31
[24] T.D. Lee, Discrete mechanics, Erice Lecture Notes, 1981
[25] H.W. Hamber and R.M. Williams, Nucl. Phys. B248 (1984) 392; Phys. Lett. 157B (1985) 368
[26] B. Berg, Phys. Rev. Lett. 55 (1985) 904; Tallahassee preprint FSU-SCRI-86-03
[27] D.V. Boulatov, V.A. Kazakov, I.K. Kostov and A.A. Migdal, Phys. Lett. B, to be published